Monthly Notices
of the
ROYAL ASTRONOMICAL SOCIETY

Mon. Not. R. Astron. Soc. **408,** 992–998 (2010) doi:10.1111/j.1365-2966.2010.17165.x

Two new hot subdwarf binaries in the *GALEX* survey

A. Kawka,[1⋆]† S. Vennes,[1⋆]† P. Németh,[2⋆] M. Kraus[1⋆] and J. Kubát[1⋆]

[1]*Astronomický ústav, Akademie věd České republiky, Fričova 298, CZ-251 65 Ondřejov, Czech Republic*
[2]*Department of Physics and Space Sciences, Florida Institute of Technology, 150 West University Boulevard, Melbourne, FL 32901-6975, USA*

Accepted 2010 June 8. Received 2010 June 4; in original form 2010 May 16

ABSTRACT

We report the discovery of two new hot, hydrogen-rich subdwarfs (sdB) in close binary systems. The hot subdwarfs, GALEX J0321+4727 and GALEX J2349+3844, were selected from a joint optical–ultraviolet catalogue of hot subluminous stars based on GSC2.3.2 and the *Galaxy Evolution Explorer* all-sky survey. Using high-dispersion spectra of the Hα core, obtained using the 2-m telescope at Ondřejov Observatory, we measured the radial velocities of the sdB primaries and determined orbital periods of 0.265 84±0.000 04 d and 0.462 49±0.000 07 d for GALEX J0321+4727 and GALEX J2349+3844, respectively. The time series obtained from the Northern Sky Variability Survey with an effective wavelength near the *R*-band show that GALEX J0321+4727 is a variable star ($\Delta m = 0.12$ mag), while no significant variations are observed in GALEX J2349+3844. The period of variations in GALEX J0321+4727 coincides with the orbital period and the variability is probably caused by a reflection effect on a late-type secondary star. Lack of photometric variations in GALEX J2349+3844 probably indicates that the companion is a white dwarf star. Using all available photometry and spectroscopy, we measured the atmospheric properties of the two sdB stars and placed limits on the mass and luminosity of the companion stars.

Key words: binaries: close – binaries: spectroscopic – subdwarfs.

1 INTRODUCTION

Subdwarf B (sdB) stars are helium core burning stars with very thin hydrogen envelopes that lie at the blue end of the horizontal branch and hence are identified with the extreme horizontal branch (EHB) stars (see a recent review by Heber 2009). D'Cruz et al. (1996) showed that a high mass-loss rate on the red giant branch produces a thin hydrogen envelope and prevents the star from ascending the asymptotic giant branch. The evolution of single EHB stars from zero age to helium exhaustion may be followed on a series of tracks narrowly centred on 0.475 $M_\odot$ (Dorman, Rood & O'Connell 1993). After helium exhaustion these objects evolve directly on to the white dwarf sequence.

On the other hand, following the original proposal of Mengel, Norris & Gross (1976) for the formation of sdB stars through binary evolution, it has been found that a significant fraction of these stars resides in close binary systems (e.g. Maxted et al. 2001; Morales-Rueda et al. 2003). The onset of a common envelope (CE) phase or Roche lobe overflow (RLOF) contributes to the removal of the hydrogen envelope and directs the star towards the EHB. Han et al. (2002, 2003) propose three formation channels for the formation of sdB stars through binary interaction, either involving CE phases, episodes of RLOF, or the merger of two helium white dwarfs. The CE scenario involving primary stars that experience a helium flash accompanied by a low-mass or white dwarf secondary star is expected to create short-period binaries [$\log P$ (d) ≈ -1 to 1] and a final primary mass distribution narrowly centred on 0.46 $M_\odot$. The CE scenario with primary stars massive enough to avoid a helium flash is expected to achieve a much lower final mass for the primary (0.33–0.35 $M_\odot$). On the other hand, the RLOF scenario creates longer period binaries and a wider distribution of primary final masses. Studies of the binary components, and an estimate of the frequency of such systems, are required to constrain these models and determine the relative contribution of these formation channels to the sdB population.

In this context, we have initiated a program to identify new hot subdwarf candidates (Vennes et al., in preparation). We combined ultraviolet photometric measurements from the *Galaxy Ultraviolet Explorer* (*GALEX*) all-sky survey and photographic visual magnitudes from the Guide Star Catalog, Version 2.3.2 (GSC2.3.2), to build a list of blue stellar candidates, while follow-up spectroscopic measurements further constrained the properties of the candidates. In Section 2, we present available spectroscopic and photometric

⋆E-mail: kawka@sunstel.asu.cas.cz (AK); vennes@sunstel.asu.cas.cz (SV); pnemeth@fit.edu (PN); kraus@sunstel.asu.cas.cz (MK); kubat@sunstel.asu.cas.cz (JK)

†Visiting Astronomer, Kitt Peak National Observatory, National Optical Astronomy Observatory, which is operated by the Association of Universities for Research in Astronomy (AURA) under cooperative agreement with the National Science Foundation.

Table 1. Astrometry and photometry.

	J0321+4727	J2349+3844
RA (2000)	03 21 39.629	23 49 47.645
Dec. (2000)	+47 27 18.79	+38 44 41.57
$\mu_\alpha \cos\delta$ (Tycho-2)	57.2 ± 1.9 mas yr^{-1}	-7.5 ± 3.5 mas yr^{-1}
μ_δ (Tycho-2)	-8.5 ± 1.8 mas yr^{-1}	1.6 ± 3.2 mas yr^{-1}
$\mu_\alpha \cos\delta$ (UCAC3)	58.0 ± 1.0 mas yr^{-1}	-4.0 ± 2.3 mas yr^{-1}
μ_δ (UCAC3)	-8.4 ± 1.0 mas yr^{-1}	-1.4 ± 1.3 mas yr^{-1}
FUV	12.441 ± 0.019	11.261 ± 0.021
NUV	11.913 ± 0.007	11.310 ± 0.005
B	11.53 ± 0.11	11.66 ± 0.11
V	11.72 ± 0.16	11.72 ± 0.15
2MASS *J*	11.807 ± 0.023	12.040 ± 0.024
2MASS *H*	11.859 ± 0.030	12.156 ± 0.031
2MASS *K*	11.893 ± 0.029	12.184 ± 0.024

measurements of two new, hot sdB stars. Section 3 presents our analysis of the radial-velocity measurements, and in Section 4 we constrain the properties of the binary components. We summarize and conclude in Section 5.

2 OBSERVATIONS

The ultraviolet sources GALEX J234947.7+384440 (hereafter GALEX J2349+3844) and GALEX J032139.8+472716 (hereafter GALEX J0321+4727) were originally selected based on the colour index $NUV - V < 0.5$ and the brightness limit $NUV < 14$, where *NUV* is the *GALEX* near-ultraviolet bandpass and *V* is the GSC photographic magnitude. The sources were also identified with optical counterparts in the Tycho-2 catalogue (Høg et al. 2000) and the Third US Naval Observatory CCD Astrograph Catalog (UCAC3; Zacharias et al. 2010). GALEX J0321+4727 is also known as a disqualified member (No. 488) of the cluster Melotte 20 (see Mermilliod, Queloz & Mayor 2008; van Leeuwen 2009). Heckmann, Dieckvoss & Knox (1956) listed a spectral type of B7 but excluded it as a possible cluster member based on its proper motion. GALEX J2349+3844 was independently identified in the First Byurakan Survey of Blue Stellar Objects as FBS 2347+385 (Mickaelian 2008).

2.1 Photometry and astrometry

We extracted the ultraviolet photometry from the *GALEX* all-sky survey using CasJobs at the Multimission Archive at STScI (MAST). *GALEX* obtained photometric measurements in the *FUV* and *NUV* bands with effective wavelengths of 1528 and 2271 Å, respectively. We corrected the photometry for non-linearity (Morrissey et al. 2007). Although the statistical errors are small ($<$0.02 mag) we estimate the total errors to be $\gtrsim$0.2 mag because of large uncertainties in the linearity corrections for bright sources (see Morrissey et al. 2007). In the present case, the *NUV* measurements are more reliable than the *FUV* measurements. We also obtained infrared photometry from the Two Micron All Sky Survey (2MASS; Skrutskie et al. 2006) and optical photometry from the Tycho catalogue.[1] We transformed the Tycho B_T and V_T photometric magnitudes to the Johnson *B* and *V* magnitudes using the recommended transformation equations (Perryman 1997).

Table 1 lists the available photometry for the two sources and astrometric measurements from Tycho-2 and UCAC3. The tabulated coordinates (epoch and equinox 2000) are the averages of the Tycho-2 and UCAC3 coordinates. Both optical counterparts lie within $\sim$3 arcsec of the ultraviolet sources.

Finally, we have extracted photometry from the Northern Sky Variability Survey (NSVS). The photometric bandpass is very broad, ranging from 4500 to 10 000 Å, with an effective wavelength close to the Johnson *R* band (Woźniak 2004). The Modified Julian Dates supplied by NSVS were converted to the Barycentric Julian Dates. The time series comprise 173 and 240 good measurements for GALEX J0321+4727 and GALEX J2349+3844, respectively, and allow the examination of our objects for variability. We also obtained a photometric series (167 good measurements) of the known eclipsing and variable sdB+dM binary 2M 1533+3759 (For et al. 2010) to test our methodology.

2.2 Spectroscopy

We observed GALEX J2349+3844 and GALEX J0321+4727 using the spectrograph at the coudé focus of the 2-m telescope at Ondřejov Observatory (Šlechta & Škoda 2002). We obtained the spectroscopic series using the 830.77 lines mm^{-1} grating with a SITe 2030 $\times$ 800 CCD that delivered a spectral resolution $R = 13\,000$ and a spectral range from 6254 to 6763 Å. The exposure time for both targets was 30 min, with each exposure immediately followed by a ThAr comparison arc. The fast rotating B star HR 7880 was observed each night to help remove telluric features from the spectra. We verified the stability of the wavelength scale by measuring the wavelength centroids of O I sky lines. The velocity scale remained stable within 1 km s^{-1}.

We also obtained two low-dispersion spectra of GALEX J0321+4727 using the Ritchey–Chretien (RC) spectrograph attached to the 4-m telescope at Kitt Peak National Observatory (KPNO) on UT 2010 March 23. We used the KPC-10A grating (316 lines mm^{-1}) with the WG360 order blocking filter. The slit width was set to 1.5 arcsec to provide a resolution of full width at half-maximum (FWHM) of 5.5 Å. A HeNeAr comparison spectrum was obtained following the target spectrum. We exposed GALEX J0321+4727 for 60 and 180 s and we co-added the spectra weighted by the exposure times. All spectra were reduced using standard procedures within IRAF.

3 BINARY PARAMETERS

3.1 Radial-velocity variations

We measured the radial velocities by fitting a Gaussian function to the Hα core and by measuring the shifts relative to the rest wavelength. The shifts were then converted into radial velocities and adjusted to the Solar system barycentre. Tables 2 and 3 list the Barycentric Julian Dates, radial velocities and the spectra signal-to-noise ratios (S/N values) for GALEX J0321+4727 and GALEX J2349+3844, respectively. The accuracy of individual measurements varied from 1 km s^{-1} in high-S/N spectra to 10 km s^{-1} in lower quality spectra.

The orbital parameters were determined by fitting to the velocity series a sinusoidal function of the form

$$v(t) = \gamma + K \sin(2\pi[t - T_0]/P),$$

where P is the period, γ is the systemic velocity, K is the velocity semi-amplitude and T_0 is the initial epoch. The initial epoch T_0 corresponds to the inferior conjunction of the sdB ($\Phi = 0$).

[1] Accessed at VizieR (Ochsenbein, Bauer & Marcout 2000).

Table 2. Radial velocities of GALEX J0321+4727.

BJD (245 5000+)	v (km s^{-1})	S/N	BJD (245 5000+)	v (km s^{-1})	S/N
45.543 17	+24.9	29	75.613 81	+38.6	13
45.574 95	+61.4	32	76.408 49	+66.1	20
59.494 49	+119.6	25	76.431 66	+86.7	21
62.587 12	+58.9	15	76.454 73	+112.2	22
62.610 18	+95.5	10	76.477 82	+120.4	22
63.557 02	+45.3	10	76.495 89	+120.9	11
63.579 98	+13.8	15	76.526 87	+95.7	14
63.602 93	+15.1	17	76.549 89	+80.6	15
63.615 45	+13.7	12	76.573 03	+49.1	14
75.410 35	+143.4	15	84.566 26	+35.5	13
75.433 22	+131.9	18	84.590 55	+9.4	26
75.486 07	+82.6	15	84.613 63	+12.2	24
75.509 93	+46.0	13	84.636 84	+35.0	25
75.533 28	+14.5	16	98.383 56	+18.2	8
75.590 48	+28.1	13			

Table 3. Radial velocities of GALEX J2349+3844.

BJD (245 5000+)	v (km s^{-1})	S/N	BJD (245 5000+)	v (km s^{-1})	S/N
45.485 74	−32.6	21	75.563 57	−4.7	12
45.507 00	+2.0	22	76.316 84	−47.6	17
59.405 94	+29.0	25	76.339 94	−71.0	18
62.499 09	−62.8	8	76.361 23	−82.4	16
63.461 12	−76.3	15	76.384 63	−79.2	20
63.484 09	−70.0	18	84.289 86	−74.6	25
63.513 35	−41.2	17	84.312 70	−61.3	26
63.536 34	−10.2	17	84.335 75	−38.1	27
68.422 25	−19.7	14	84.358 98	−8.4	25
68.465 53	−55.4	12	84.381 79	+38.6	27
69.351 58	−31.8	14	84.404 64	+54.1	27
69.378 13	−52.8	19	84.427 47	+78.3	30
69.402 26	−67.9	9	84.450 30	+86.0	23
70.508 80	+23.4	18	84.473 49	+86.9	19
70.532 08	+56.3	27	84.496 79	+86.4	22
74.538 54	−97.6	13	84.520 89	+68.0	24
75.318 18	+26.7	18	84.543 75	+53.4	25
75.341 17	+2.9	15	98.291 11	+59.4	17
75.363 93	−20.4	18	98.314 03	+76.7	16
75.388 21	−38.7	15	98.337 09	+90.4	17
75.465 18	−81.3	11	98.360 17	+78.5	10

We applied a χ^2 minimization technique with each velocity measurement weighted proportionally to the S/N achieved in the corresponding spectrum. Figs 1 and 2 show the periodograms and the best-fitting radial-velocity curves for GALEX J0321+4727 and GALEX J2349+3844, respectively. The residual to the best-fitting radial curve is ≈6 km s^{-1} for both data sets. Table 4 lists the corresponding binary parameters and the calculated mass functions. The measured radial velocities were also employed to apply Doppler corrections to individual spectra and build phase-averaged spectra for each star (Section 4).

Our new systemic velocity for GALEX J0321+4727 (γ = 70.5 km s^{-1}) also clearly rules out membership to the cluster Melotte 20 ($\gamma = -1.4$ km s^{-1}; Mermilliod et al. 2008).

3.2 Photometric variations

We investigated possible variability in GALEX J0321+4727 and GALEX J2349+3844 using the NSVS light curves. We analyse

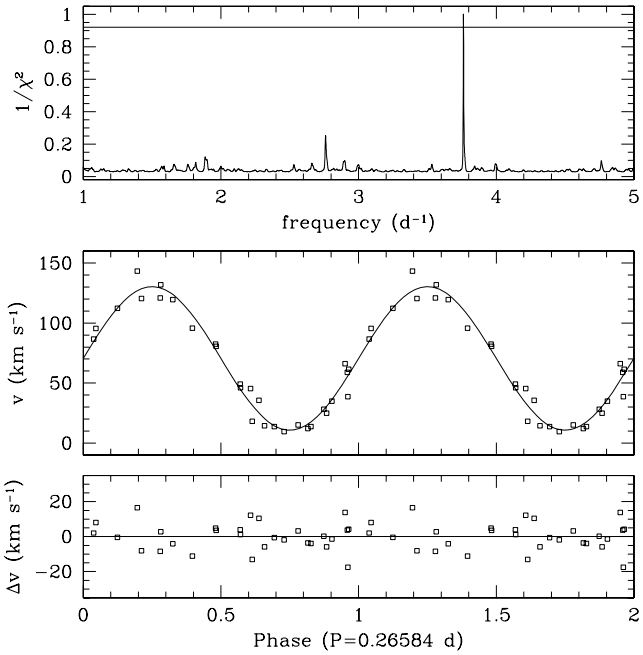

Figure 1. Top panel: period analysis of GALEX J0321+4727 showing a single significant period. Middle panel: radial-velocity measurements folded on the orbital period and the best-fitting sine curve. Bottom panel: residual of the velocities relative to the best-fitting sine curve.

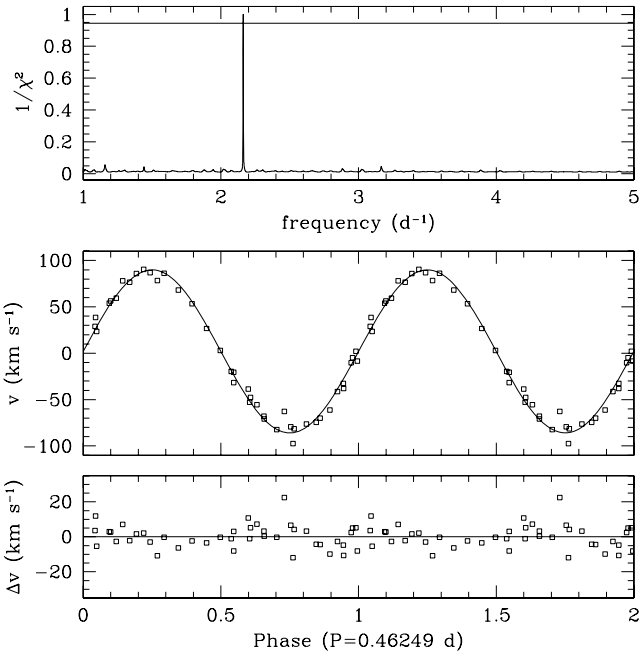

Figure 2. Same as Fig. 1 but for GALEX J2349+3844.

Table 4. Binary parameters.

Parameter	J0321+4727	J2349+3844
Period (d)	0.265 84 ± 0.000 04	0.462 49 ± 0.000 07
T_0 (BJD 245 5000+)	45.582 ± 0.011	45.511 ± 0.013
K (km s^{-1})	59.8 ± 4.5	87.9 ± 2.2
γ (km s^{-1})	70.5 ± 2.2	2.0 ± 1.0
$f(M_{\rm sec})$ ($M_\odot$)	0.005 89 ± 0.000 15	0.032 54 ± 0.000 44

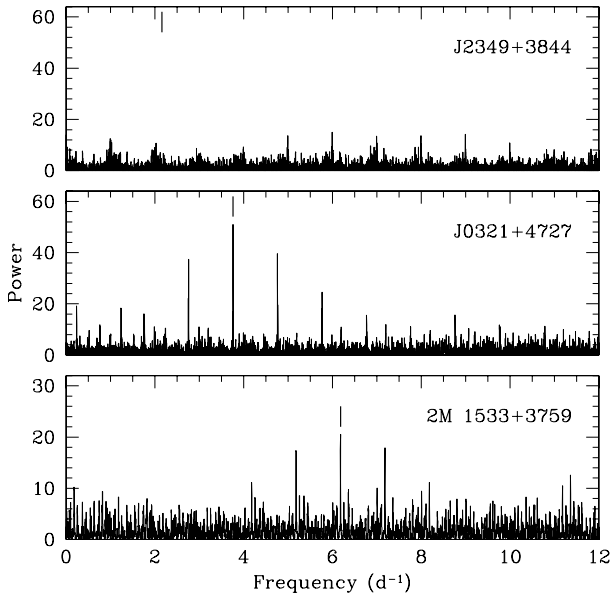

Figure 3. Lomb periodograms of GALEX J0321+4727 and GALEX J2349+3844 and the test target 2M 1533+3759.

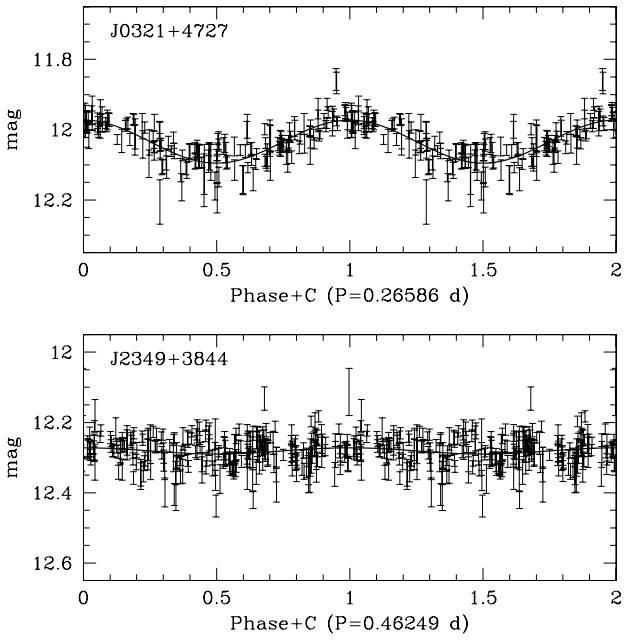

Figure 4. NSVS light curves of GALEX J0321+4727 and GALEX J2349+3844 compared to the best-fitting sine curves with semi-amplitudes of 0.061 ± 0.004 and 0.009 ± 0.004 mag, respectively.

the light curves using a Lomb periodogram for unevenly sampled time series (Press et al. 1992). The power spectra (Fig. 3) show a peak signal at a frequency close to the orbital period in GALEX J0321+4727 (Table 4) and 2M 1533+3759 (For et al. 2010), but not in GALEX J2349+3844 (Table 4). We estimated the probability of a given frequency relative to the probability of the peak frequency following Press et al. (1992) and determined the 1σ (66 per cent) error bars on the period of the photometric variations for GALEX J0321+4727,

$$P = 0.265\,86 \pm 0.000\,03 \text{ d},$$

and for 2M 1533+3759,

$$P = 0.161\,77 \pm 0.000\,03 \text{ d}.$$

For both stars, the period of photometric variations is equal, within error bars, to the measured orbital period, thereby validating the method. Fig. 4 shows the NSVS light curves for GALEX J0321+4727 and GALEX J2349+3844 folded on the orbital period with an arbitrary phase adjustment so that $\Phi = 0$ corresponds to the inferior conjunction of the primary star (sdB). The distant NSVS epoch (1999) precluded phasing with the current orbital ephemeris (Table 4). The light curve of GALEX J0321+4727 is fitted with the sine curve

$$m = (12.034 \pm 0.003) + (0.061 \pm 0.004)\ \sin 2\pi\Phi,$$

which we interpret as a reflection effect on a late-type secondary star (Section 4). The variations in GALEX J2349+3844 are not significant with a mean magnitude of $\langle m \rangle = 12.281 \pm 0.003$ and a semi-amplitude of $\Delta m/2 = 0.009 \pm 0.004$.

4 PROPERTIES OF THE COMPONENTS

Our analysis of the spectroscopic observations of the primary stars is based on a grid of non-local thermodynamic equilibrium (non-LTE) models and synthetic spectra calculated using TLUSTY/SYNSPEC (Hubeny & Lanz 1995; Lanz & Hubeny 1995). The grid covers the effective temperature from $T_{\rm eff} = 21\,000$ to $35\,000$ K (in steps of 1000 K), the surface gravity from $\log g = 4.75$ to 6.25 (in steps of 0.25) and the helium abundance from $\log(n_{\rm He}/n_{\rm H}) = -4.0$ to -1.0 (in steps of 0.5). The neutral hydrogen and helium atoms include 9 ($n \leq 9$) and 24 ($n \leq 8$) energy levels, respectively, and the ionized helium atom includes 20 ($n \leq 20$) energy levels.

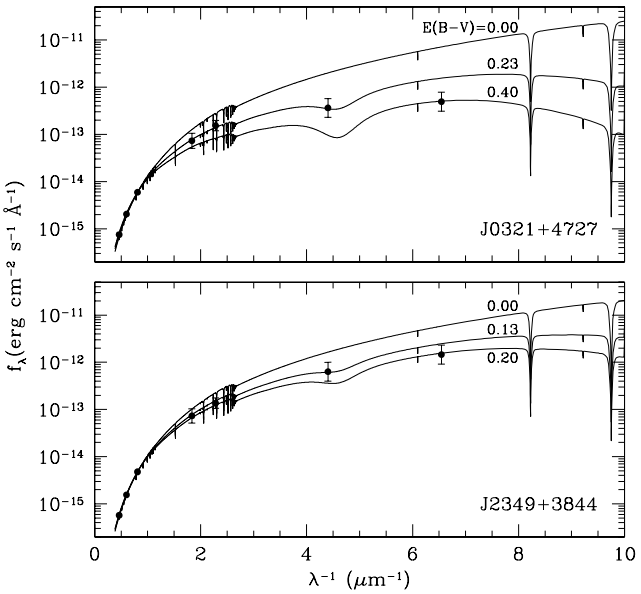

Figure 5. Top panel: spectral energy distribution of GALEX J0321+4727 compared to a model spectrum that was corrected for interstellar extinction assuming $E(B-V) = 0.0, 0.23, 0.4$ and $R_V = 3.2$. Bottom panel: same but for GALEX J2349+3844 and assuming $E(B-V) = 0.0,\ 0.13$ and 0.2.

4.1 Spectral energy distribution

Fig. 5 shows a preliminary analysis of the atmospheric properties of the two sdB stars using their observed spectral energy distribution (SED) from the infrared to the ultraviolet, and using representative

sdB models at $T_{\rm eff} = 29\,000$ K, $\log g = 5.5$ and $\log(n_{\rm He}/n_{\rm H}) = -2.65$ (GALEX J0321+4727) and -3.25 (GALEX J2349+3844). The model corresponds to a hot sdB star with absolute magnitude $M_V = 4.1$ and a canonical mass of $0.47\,{\rm M}_{\odot}$ (see Dorman et al. 1993). We corrected the model spectra for interstellar extinction using a variable extinction coefficient $E(B-V)$ and a parametrized extinction law ($R = 3.2$; Cardelli, Clayton & Mathis 1989). GALEX J0321+4727 lies close to the plane of the Galaxy ($l = 147.5$, $b = -8.1$) and the total extinction in the line of sight is $E(B-V) = 0.61$ (Schlegel, Finkbeiner & Davis 1998). Excluding the *FUV* band, the observed SED is well matched by the model assuming $E(B-V) = 0.23$. A much higher coefficient ($\approx$0.4) is required to match the *FUV* band although the accuracy of the *FUV* photometry is most probably affected by non-linearity (see Section 2.1). GALEX J2349+3844 is located below the plane ($l = 110.0$, $b = -22.6$) and the total extinction is lower $E(B-V) = 0.17$. In this case, the SED is well matched assuming $E(B-V) = 0.13$. These estimates appear reasonable if we locate both stars at a distance of $\sim$330 pc by assuming $M_V \sim 4.1$ and $V = 11.7$ for both stars. Taking the scaleheight for dust in the Galactic plane as $h \approx 150$ pc, the total distance across the dust layer is $\approx$1060 and 390 pc at $|b| = 8.1$ and $22^{\circ}.6$, respectively, so that the path towards GALEX J0321+4727 covers $\sim$31 per cent of the total distance and $\sim$85 per cent for GALEX J2349+3844. According to this simple calculation, the scaled $E(B-V)$ indices are predicted to be 0.19 and 0.15 for GALEX J0321+4727 and GALEX J2349+3844, respectively, and are similar to our estimates based on the SED.

Taking into account the effect of interstellar reddening, the entire spectral energy distribution of both systems is dominated by the sdB stars.

4.2 Line-profile analysis

We measured the sdB effective temperature ($T_{\rm eff}$), surface gravity ($\log g$) and helium abundance [$\log(n_{\rm He}/n_{\rm H})$] by fitting the observed line profiles with our grid of model spectra. We employed χ^2 minimization techniques to find the best-fitting parameters and draw contours at 66, 90 and 99 per cent significance. The model spectra were convolved with Gaussian profiles with a FWHM = 5.5 Å for the analysis of the KPNO spectra, while we adopted a FWHM = 0.66 Å that includes the effect of orbital smearing for the Ondřejov coudé spectra.

First, we analysed the KPNO spectrum of GALEX J0321+4727 (Fig. 6). We included in the analysis the Balmer line spectrum from Hα to H11 and five blue He I lines normally dominant in sdB stars. We repeated the analysis with Hα excluded and obtained the same atmospheric parameters as the analysis that included Hα. The mid-exposure time of the co-added KPNO spectrum is BJD 245 5278.595 01 corresponding to an orbital phase $\Phi = 0.51 \pm 0.03$ or close to the inferior conjunction of the secondary star. This phase also corresponds to minimum contamination to the sdB spectrum due to the reflection effect.

Next, we analysed phase-resolved Hα spectra of GALEX J0321+4727 to take into account the light contamination due to the reflection effect on the temperature measurements. This effect was notable in the analysis of the similar systems such as HS2333+3927 (Heber et al. 2004) and 2M 1533+3759 (For et al. 2010). Variations of $\approx$6000 K were observed in HS2333+3927, while weaker variations of $\approx$1000 K were observed in 2M 1533+3759. To investigate this effect in GALEX J0321+4727 we built three spectra inclusive of phases 0.0–1.0 (average), 0.35–0.65 (minimum reflection effect) and 0.85–0.15 (maximum reflection effect). Fig. 7 shows our analysis of the Hα and He I λ6678 Å line profiles in the co-added (0.0–1.0) coudé spectra of GALEX J0321+4727 and GALEX J2349+3844.

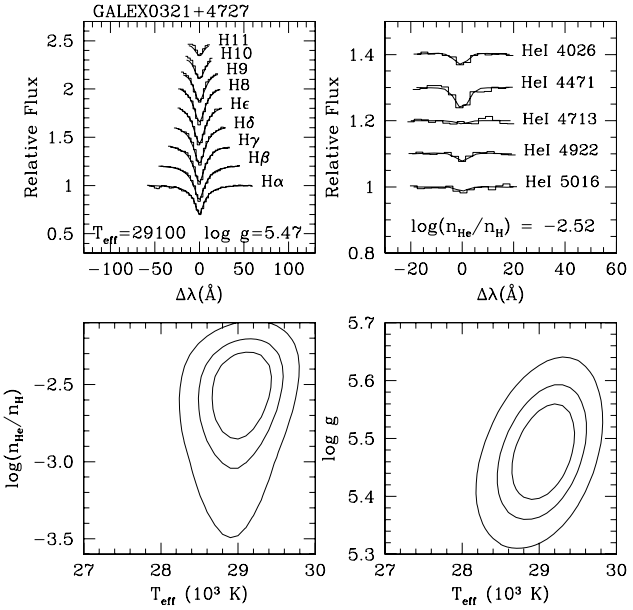

Figure 6. Model atmosphere analysis of the low-dispersion KPNO spectrum of GALEX J0321+4727. The top panels show the line profiles and the best fitting models, and the bottom panels show the χ^2 contours drawn at 66, 90 and 99 per cent.

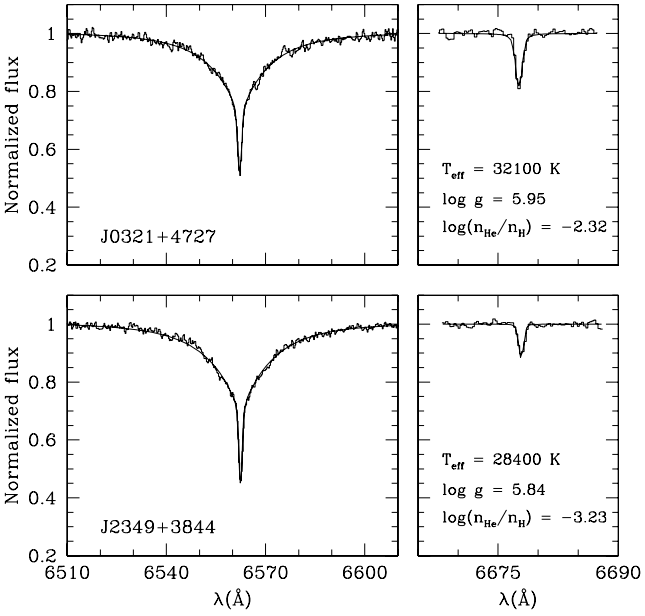

Figure 7. Co-added coudé spectra of GALEX J0321+4727 (top panel) and GALEX J2349+3844 (bottom panel) showing the Hα (left-hand panel) and He I λ6678 Å (right-hand panel) lines and the best-fitting models.

Table 5 summarizes our measurements of the hot subdwarf atmospheric parameters. Our measurements show that variability in GALEX J0321+4727 is affecting the temperature and abundance measurements but that the surface gravity does not vary significantly. In our limited phase resolution, the peak-to-peak temperature variation reaches $\approx$4000 K. The Ondřejov coudé and KPNO temperature measurements at phase 0.5 agree but the surface gravity measurements differ by 0.5 dex. This is most likely due to a

Table 5. Measurements.

Range	Phase	$T_{\rm eff}$ (K)	$\log g$ (cgs)	$\log n_{\rm He}/n_{\rm H}$
		J0321+4727		
Hα	0.85–0.15	$33\,750 \pm 350$	5.88 ± 0.07	-2.10 ± 0.10
Hα	0.00–1.00	$32\,100 \pm 250$	5.95 ± 0.05	-2.32 ± 0.07
Hα	0.35–0.65	$29\,550 \pm 650$	5.98 ± 0.09	-2.68 ± 0.20
Hα–H11	0.50	$29\,100 \pm 350$	5.47 ± 0.08	$-2.52^{+0.22}_{-0.31}$
		J2349+3844		
Hα	0.00–1.00	$28\,400 \pm 400$	5.84 ± 0.06	-3.23 ± 0.09

systematic effect in the model spectra themselves with the Hα line-profile analysis overestimating the surface gravity relative to an analysis involving the complete series. The shape and strength of the upper Balmer lines are very sensitive to surface gravity and offer a more reliable surface gravity diagnostics. In summary we estimate the parameters representative of the sdB GALEX J0321+4727 at phase 0.5. The effective temperature and helium abundance were estimated by taking the weighted average of the results from the Hα–H11 and Hα (0.35–0.65) fits and for the surface gravity we adopted the result from the Hα–H11 analysis:

$$T_{\rm eff} = 29\,200 \pm 300, \quad \log g = 5.5 \pm 0.1$$

and

$$\log n_{\rm He}/n_{\rm H} = -2.6 \pm 0.1.$$

Applying a correction of -0.5 ± 0.2 to the surface gravity measurement of GALEX J2349+3844 that is based on Hα alone, we conservatively estimate the sdB parameters:

$$T_{\rm eff} = 28\,400 \pm 400, \quad \log g = 5.4 \pm 0.3$$

and

$$\log n_{\rm He}/n_{\rm H} = -3.2 \pm 0.1.$$

Our analysis assumes a hydrogen/helium composition and the inclusion of heavy elements in the model atmospheres is likely to affect our results (see Heber, Reid & Werner 2000; Edelmann et al. 2003). A self-consistent analysis including abundance measurements (e.g. O'Toole & Heber 2006; Ahmad et al. 2007) awaits high-S/N and high-resolution ultraviolet and optical spectroscopy.

4.3 Nature of the companions

Using the mass function (Table 4) and assuming a mass of $0.5\,{\rm M}_{\odot}$ for the hot subdwarf GALEX J0321+472, we calculate a minimum secondary mass of $0.13\,{\rm M}_{\odot}$ that corresponds to a spectral type of M5 (Kirkpatrick & McCarthy 1994). Assuming an absolute J magnitude of 3.9 for the hot subdwarf, a M5 star with $M_J = 8.8$ would be outshone by the hot subdwarf.

The NSVS light curve shows GALEX J0321+4727 to be variable and the search for a period in the photometric data resulted in a best period corresponding to the orbital period. The observed variations are most probably caused by irradiation of the atmosphere of the cool companion by the hot subdwarf. Using the observed semi-amplitude of 0.061 mag we may constrain the binary parameters further. We estimated the system inclination and secondary mass using the reflection model of Maxted et al. (2002) and assumed two different masses for the sdB star. For a sdB mass of $0.4\,{\rm M}_{\odot}$, the inclination is predicted to be between 63° and 71° and the secondary mass between 0.124 and $0.133\,{\rm M}_{\odot}$. For a sdB mass of $0.5\,{\rm M}_{\odot}$, we obtain an inclination ranging from 65° to 70°, and a secondary mass between 0.143 and $0.149\,{\rm M}_{\odot}$.

Again, using the mass function and assuming a mass of $0.5\,{\rm M}_{\odot}$ for the hot subdwarf GALEX J2349+3844, the minimum secondary mass is $0.27\,{\rm M}_{\odot}$ that corresponds to a spectral type of M4 (Kirkpatrick & McCarthy 1994). Assuming an absolute J magnitude of 5.6 for the hot subdwarf, a M4 spectral type star with $M_J = 8.6$ would also be outshone by the hot subdwarf.

However, the NSVS time series do not show variations down to a limit of $\Delta m = 0.009$. Illumination of a $0.3\,{\rm M}_{\odot}$ star, which is the suggested mass at a high inclination, would cause a variation of $\Delta m \sim 0.4$ mag. Lower inclinations would require larger companions causing even larger variations that are incompatible with the observations. The lack of variability suggests that the companion is most likely a white dwarf (see Maxted, Morales-Rueda & Marsh 2004).

5 SUMMARY AND CONCLUSIONS

We show that GALEX J0321+4727 and GALEX J2349+3844 are hot hydrogen-rich subdwarfs in close binaries. Based on a preliminary analysis of periodic light variations in GALEX J0321+4727, we infer that its companion is a low-mass star ($M \sim 0.13\,{\rm M}_{\odot}$). The secondary star in GALEX J2349+3844 is probably a white dwarf with $M \gtrsim 0.3\,{\rm M}_{\odot}$. The two new systems are post-CE systems with a hot subdwarf primary. Their orbital periods locate them close to the peak of the period distribution for such systems (see Heber 2009). A future study of GALEX J0321+4727 will involve phase-resolved high-S/N spectroscopic and photometric observations aimed at resolving the nature of the companion. Searches for close binaries in the sdB population have a relatively high yield (69 per cent; see Maxted et al. 2001), and, therefore, we expect that many new systems remain to be discovered in our *GALEX*/GSC catalogue of EHB stars.

ACKNOWLEDGMENTS

SV and AK are supported by GA AV grant numbers IAA300030908 and IAA301630901, respectively, and by GA ČR grant number P209/10/0967. AK also acknowledges support from the Centre for Theoretical Astrophysics (LC06014). Some of the data presented in this paper were obtained from the Multimission Archive at the Space Telescope Science Institute (MAST). STScI is operated by the Association of Universities for Research in Astronomy, Inc., under NASA contract NAS5-26555. Support for MAST for non-*HST* data is provided by the NASA Office of Space Science via grant NNX09AF08G and by other grants and contracts.

REFERENCES

Ahmad A., Behara N. T., Jeffery C. S., Sahin T., Woolf V. M., 2007, A&A, 465, 541
Cardelli J. A., Clayton G. C., Mathis J. S., 1989, ApJ, 345, 245
D'Cruz N. L., Dorman B., Rood R. T., O'Connell R. W., 1996, ApJ, 466, 359
Dorman B., Rood R. T., O'Connell R. W., 1993, ApJ, 419, 596
Edelmann H., Heber U., Hagen H.-J., Lemke M., Dreizler S., Napiwotzki R., Engels D., 2003, A&A, 400, 939
For B.-Q. et al., 2010, ApJ, 708, 253
Han Z., Podsiadlowski Ph., Maxted P. F. L., Marsh T. R., Ivanova N., 2002, MNRAS, 336, 449
Han Z., Podsiadlowski Ph., Maxted P. F. L., Marsh T. R., 2003, MNRAS, 341, 669

Heber U., 2009, ARA&A, 47, 211
Heber U., Reid I. N., Werner K., 2000, A&A, 363, 198
Heber U. et al., 2004, A&A, 420, 251
Heckmann V. O., Dieckvoss W., Knox H., 1956, Astron. Nachr., 283, 109
Høg E. et al., 2000, A&A, 355, L27
Hubeny I., Lanz T., 1995, ApJ, 439, 875
Kirkpatrick J. D., McCarthy D. W., Jr, 1994, AJ, 107, 333
Lanz T., Hubeny I., 1995, ApJ, 439, 905
Maxted P. F. L., Heber U., Marsh T. R., North R. C., 2001, MNRAS, 326, 1391
Maxted P. F. L., Marsh T. R., Heber U., Morales-Rueda L., North R. C., Lawson W. A., 2002, MNRAS, 333, 231
Maxted P. F. L., Morales-Rueda L., Marsh T. R., 2004, Ap&SS, 291, 307
Mengel J. G., Norris J., Gross P. G., 1976, ApJ, 204, 488
Mermilliod J.-C., Queloz D., Mayor M., 2008, A&A, 488, 409
Mickaelian A. M., 2008, AJ, 136, 946
Morales-Rueda L., Maxted P. F. L., Marsh T. R., North R. C., Heber U., 2003, MNRAS, 338, 752
Morrissey P. et al., 2007, ApJS, 173, 682
Ochsenbein F., Bauer P., Marcout J., 2000, A&AS, 143, 23
O'Toole S. J., Heber U., 2006, A&A, 452, 579
Perryman M. A. C., 1997, The Hipparcos and Tycho Catalogues, ESA SP-1200. ESA, Noordwijk
Press W. H., Teukolsky S. A., Vetterling W. T., Flannery B. P., 1992, Numerical Recipes in FORTRAN. The Art of Scientific Computing, 2nd edn. Cambridge Univ. Press, Cambridge
Schlegel D. J., Finkbeiner D. P., Davis M., 1998, ApJ, 500, 525
Skrutskie M. F. et al., 2006, AJ, 131, 1163
Šlechta M., Škoda P., 2002, Publ. Astron. Inst. Acad. Sci. Czech Republic, 90, 1
van Leeuwen F., 2009, A&A, 497, 209
Woźniak P. R. et al., 2004, AJ, 127, 2436
Zacharias N. et al., 2010, AJ, 139, 2184

This paper has been typeset from a TEX/LATEX file prepared by the author.